RESEARCH

Attenuated total reflection Fourier-transform infrared spectroscopy reveals environment specific phenotypes in clonal Japanese knotweed

Claire A. Holden[1*], Martin McAinsh[1], Jane E. Taylor[1], Paul Beckett[2] and Francis L. Martin[3,4]

Abstract

Background Japanese knotweed (*Reynoutria japonica* var. *japonica*), a problematic invasive species, has a wide geographical distribution. We have previously shown the potential for attenuated total reflection Fourier-transform infrared (ATR-FTIR) spectroscopy and chemometrics to segregate regional differentiation between Japanese knotweed plants. However, the contribution of environment to spectral differences remains unclear. Herein, the response of Japanese knotweed to varied environmental habitats has been studied. Eight unique growth environments were created by manipulation of the red: far-red light ratio (R: FR), water availability, nitrogen, and micronutrients. Their impacts on plant growth, photosynthetic parameters, and ATR-FTIR spectral profiles, were explored using chemometric techniques, including principal component analysis (PCA), linear discriminant analysis, support vector machines (SVM) and partial least squares regression. Key wavenumbers responsible for spectral differences were identified with PCA loadings, and molecular biomarkers were assigned. Partial least squared regression (PLSR) of spectral absorbance and root water potential (RWP) data was used to create a predictive model for RWP.

Results Spectra from plants grown in different environments were differentiated using ATR-FTIR spectroscopy coupled with SVM. Biomarkers highlighted through PCA loadings corresponded to several molecules, most commonly cell wall carbohydrates, suggesting that these wavenumbers could be consistent indicators of plant stress across species. R: FR most affected the ATR-FTIR spectra of intact dried leaf material. PLSR prediction of root water potential achieved an R2 of 0.8, supporting the potential use of ATR-FTIR spectrometers as sensors for prediction of plant physiological parameters.

Conclusions Japanese knotweed exhibits environmentally induced phenotypes, indicated by measurable differences in their ATR-FTIR spectra. This high environmental plasticity reflected by key biomolecular changes may contribute to its success as an invasive species. Light quality (R: FR) appears critical in defining the growth and spectral response to environment. Cross-species conservation of biomarkers suggest that they could function as indicators of plant-environment interactions including abiotic stress responses and plant health.

*Correspondence:
Claire A. Holden
c.holden6@lancaster.ac.uk

Full list of author information is available at the end of the article

Introduction

In the current period of unprecedented global environmental change, the negative effects of invasive alien species (IAS) are compounded [1–4]. They are a major driver of ecosystem degradation [5, 6], and can trigger complex socio-economic problems affecting human livelihoods and well-being [7–9]. Effective establishment in a non-native environment by IAS is partly dependent on their ability to compete with native flora for key resources (light, nutrients, and water), the availability of which is limited [10, 11]. Human interference is creating new environments such as those with fluctuating water availability [12] and high nitrogen ecosystems [13]. Whilst native plants may be more able to withstand drought [14], the versatility of IAS frequently earns them the advantage. As opportunists, a non-uniform distribution of nutrients often increases the competitive edge of invasive plants [14]. Japanese knotweed is an opportunistic invasive species that is well-known for its expensive eradication and impact on property values in the United Kingdom [15]. It is able to take advantage of fluctuating resources, perhaps because its nitrogen-use efficiency is superior to that of native plants [16]. Increased nitrogen availability exacerbates the impacts of invasive species on non-native species in aboveground competition [17], although nitrogen does not influence the consequences in belowground competition [18]. As an economically important weed, data on the growth response of Japanese knotweed under differing environmental conditions is of interest and was recently listed as a point of action in a Science and Technology Committee Report [19]. Invasive species may also respond to abiotic stress differently than native species, for example, Japanese knotweed is known to be very tolerant to abiotic stress, occupying extreme environments such as salt marshes [20] and metal-polluted soil [21, 22]. It has successfully achieved a wide geographical distribution and colonises diverse habitats such as riparian wetlands, urban transport courses, and coastal areas [23, 24]. Despite this variation in habitat, it exhibits minimal genetic variation in Central Europe [23], Norway [25] and the USA [24], and exists as a female clone in the United Kingdom from a single introduction [26, 27]. Phenotypic plasticity [28–35], efficient resource partitioning [36] and vegetative regeneration [37] allow clonal species such as Japanese knotweed to take advantage of a wide ecological niche regardless of their low genetic diversity.

A spectrochemical method, attenuated total reflection Fourier-transform infrared (ATR-FTIR) spectroscopy, followed by chemometrics has been successfully applied to investigate plant response to abiotic [38–43] and biotic factors [44], as well as for monitoring plant health and development [45, 46]. In combination with chemometric techniques, such as support vector machines, the multivariate spectral dataset produced through infrared spectroscopy allows the rapid, marker-free, non-destructive analysis of biological samples [47]. The mid-infrared spectral profiles of plants from different growing regions can be distinguished with chemometric techniques despite the lack of genetic diversity in Japanese knotweed [48]. The relation between environment and differences in mid-infrared spectral profiles has allowed the differentiation of plants, pollen, and plant products from different growing areas in numerous species [48–53]. Mid-infrared spectroscopy uses the absorption pattern of mid-infrared light by a sample to gain biochemical information. When light is passed through a sample, the chemical bonds within it absorb light energy at specific wavelengths (2.5–25 μm wavelengths or 4000–400 cm^{-1} wavenumbers). These wavelengths match the energy required to cause the different functional groups present in the sample to vibrate. When the light that has passed through the sample is measured, these wavelengths will not be present, as they have been absorbed by the sample. This information can be displayed as an absorbance spectrum [47]. Biological materials preferentially absorb light in the region of 1800–900 cm^{-1} wavenumbers, known as the fingerprint region, which includes important information about key biomolecules such as lipids, proteins, nucleic acids, and carbohydrates [47].

Although the biochemical differences induced by plant-environment interactions can be detected by spectral analysis that allows discrimination between plants of different growing environments, it is not known which aspects of environmental conditions have the greatest impact on plant spectral profiles. Here, a controlled study was performed to unpick which environmental factors have the greatest influence over spectral profiles of Japanese knotweed grown in eight unique environments which differ in red: far-red light ratio (R: FR), and the availability of water, nitrogen, and micronutrients, whilst maintaining comparative temperature, humidity, and photoperiod. This study indicated that the light environment, in terms of the R: FR ratio, plays a key role in shaping the spectral profile of Japanese knotweed. Spectral differences between plants of different treatment groups allowed the identification of several biomarkers of environmental effects, highlighting changes in compounds such as cell wall carbohydrates. We hypothesise that wavenumbers which are conserved between species

could be used as indicators of plant health under abiotic stress.

Materials and methods

Plant growth.

With permission from Lancashire County Council, Japanese knotweed rhizomes were extracted from Scorton Picnic Site, Preston, Lancashire, United Kingdom, PR3 1BU, before transportation to Lancaster Environment Centre. The presence of Japanese knotweed at this site was identified by Thomas Myerscough of the Wyre Rivers Trust and this species identity was confirmed by Claire A Holden of Lancaster University. Ninety fragments of rhizome (10–50 g, volume 2–58 cm^3) were planted in fertilized organic loam (John Innes No. 1, J. Arthur Bowers, UK) in cylindrical pots designed to tightly fit in a pressure chamber (Soil Moisture Equipment Corp., Santa Barbara, CA, USA) measuring 6.5 cm in diameter and 23 cm in length, with a volume of 763.2 cm^3, and featured a stainless-steel mesh (0.7 mm aperture) at the base which assisted drainage. Pots were placed in one of two climate-controlled cabinets (Microclima 1750, Snijders Scientific BV, Netherlands) at 80% humidity, 16 h of photoperiod, and 19/11°C day/night temperature where treatments were applied and plants were grown for a total of fifty days before harvesting. The long photoperiod and temperature range were selected to simulate an average British summer in the areas Japanese knotweed usually colonises, using a comparison of temperature maps from the Met Office [54] and a distribution map of Japanese knotweed in the British Isles [55].

Treatments.

Rhizome fragments were divided into eight treatment groups to give an even split of rhizome masses in each group. The treatments applied were: Light Control 'LC', Light Drought 'LD', Light Nitrogen 'LN', Light Low Nutrient 'LLN', Shade Control 'SC', Shade Drought 'SD', Shade Nitrogen 'SN', and Shade Low Nutrient 'SLN'. In both cabinets, the light emitted from the two high-pressure sodium lamps (SON-T 400 W, Philips Lighting, Eindhoven, The Netherlands) was reduced using a LEE 209 filter (LEE Filters Worldwide, Andover, Hampshire, UK). In one cabinet, a matrix of far-red LEDs (EPILEDS, 740–745 nm) distributed in five rows 30 cm apart was used to decrease the R: FR to simulate shading (see Supplementary Figure S1 for the spectrum produced by the LEDs alone). Wavelengths emitted were measured using an UPRtek (Taiwan) PG100N light spectrometer. The combined light conditions (see Supplementary Table S1) resulted in a 'light' treatment with a R: FR of 5.6 and a 'shade' treatment with a R: FR of 0.4 (see Supplementary Figure S1 for the spectral profile). Plants were redistributed weekly within each cabinet to minimise positional effects from the LED matrix pattern. The R: FR of natural

sunlight during the day is approximately 1.15 (Smith H, 1982) and the R: FR of 0.4 in the shade treatment was chosen to replicate that found within vegetative canopies [56]. In both cases, the photosynthetic photon flux density (PPFD) was between 124.7 and 189.8 $\mu mol \cdot m^{-2} \cdot s^{-1}$ which is typical of growth cabinet studies [57–60].

Plants were regularly provided with water (75 cm^3 pot^{-1} 48 h^{-1}), apart from LD and SD in which water was withheld for 7 days prior to harvest. Once a week, four groups (LC, LD, SC, SD) were watered with 75 mL Hoagland solution to provide both nitrogen and micronutrients, see Supplementary Table S2 for details. LN and SN were fed with the commonly used agricultural dose of 50 kg ha^{-1} $year^{-1}$ [61]; this was scaled down for a pot diameter of 6.2 cm and applied across a split-dose at 21 and 23 days to prevent leaching. Groups LLN and SLN were provided only with water and received no additional nitrogen or micronutrients.

Physiological and photosynthetic measurements.

The following non-destructive measurements were taken the day prior to harvest: shoot height, number of leaves, stem diameter using a Vernier calliper, and chlorophyll concentration using Apogee chlorophyll concentration meter (Apogee Instruments Inc, Logan, Utah, USA). Preliminary observations of well-watered plants showed that stomatal conductance was maximal during the interval four to eight hours following the light switch on in the Snijder cabinets and dropped sharply after ten hours of light exposure, therefore, this interval was selected for measurements. Before measurements were taken, whole plant transpiration was calculated by comparison of initial and final pot weights. The pot surface was covered with duct tape to minimize soil evaporation and weighed twice on a precision balance to 0.01 g (Adventurer Pro AV4102, Ohaus, Thetford, UK), with the two readings a minimum of 30 min apart. Stomatal conductance was measured using an AP4 porometer (Delta-T Devices Ltd, Burwell, Cambridge, UK). A MultispeQ Beta [62] was used to measure leaf thickness and the following photosynthesis data; Phi2, PhiNPQ, PhiNO, linear electron flow, leaf temp differential, NPQt, ECSt mAU, gH^+, vH^+, PS1 active centres, PS1 open centres, PS1 over reduced centres, PS1 oxidised centres (see Supplementary Figures S2 and S3).

A total of three leaves were excised from each plant for analysis 4–8 h into the photoperiod in order to fall within a stable period of the plants' circadian rhythm. The third leaf down was selected for bio-spectroscopy of dried whole leaves. Whole leaves were dried at 37 °C for one week and stored in a dry airtight container at room temperature before analysis using ATR-FTIR spectroscopy. The fourth leaf down was placed in a humidified plastic bag and taken immediately to the pressure chamber for determination of leaf water potential (Ψ_{leaf}). Following

this, the plant was de-topped and the whole pot inserted into a pressure chamber (Model 3000F01 Plant Water Status Console, Soil Moisture Equipment Corp., Santa Barbara, CA, USA) with the stem protruding for determination of root water potential (Ψ_{root}). Leaf area was determined using a leaf area meter (model LI-3100 C; Li-Cor, Lincoln, NE, USA) and finally aboveground fresh weight was measured. These were dried at 80 °C for four days until the mass remained constant and all the moisture was assumed lost, before reweighing for aboveground dry weight.

ATR-FTIR spectral acquisition.

Whole dried leaves were analysed using a Tensor 27 FTIR spectrometer with a Helios ATR attachment (Bruker Optics Ltd, Coventry, UK). The sampling area was 250 μm x 250 μm, as defined by the diamond crystal internal reflection element (IRE). Spectral resolution was 8 cm^{-1} with two times zero-filling, giving a data-spacing of 4 cm^{-1} over the range 4000 to 400 cm^{-1}; 32 co-additions and a mirror velocity of 2.2 kHz were used for optimum signal to noise ratio. To minimise bias, an even spread of ten spectra were taken from each surface of the leaf, twenty spectra per sample, resulting in 480 spectra in total. Each dried leaf was placed on a slide with the side to be analysed facing upwards, the slide was placed on an adjustable platform and moved upwards to ensure a good and consistent contact with the IRE. A voucher specimen of the leaves used in this study has been deposited in the University of Leicester Herbarium LTR.

Data analysis.

The 'mergetool' function of an in-house developed Matlab (Mathworks, Natick, USA) toolbox called IRootLab [63, 64] was used to convert all spectral information from OPUS format to suitable files (.txt). Following this, it was necessary to pre-process the acquired spectra to improve the signal-to-noise ratio. Pre-processing corrects problems associated with random or systematic artefacts introduced during spectral acquisition and is an essential step of all spectroscopic experiments. Pre-processing and computational analysis of the data were performed using a combination of IRootLab toolbox [64] and the PLS Toolbox version 7.9.3 (Eigenvector Research, Inc., Manson, USA). The pre-processing steps applied to all spectra were firstly the selection of the spectral biochemical fingerprint region (1800–900 cm^{-1}), followed by Savitzky–Golay (SG) second differentiation (nine smoothing points) and vector normalisation. All data were mean-centred before multivariate analysis, where multiple dependant variables are observed simultaneously to determine a pattern.

Four machine learning techniques were used in this study: an unsupervised dimensionality reduction method, two supervised classification methods and one regression. The unsupervised method PCA simplifies complex multivariate datasets, allowing them to be presented intuitively and enabling pattern recognition. This process is known as dimensionality reduction. Two supervised chemometric techniques, PCA-LDA and SVM, were used for the classification of groups [65, 66]. PCA-LDA was also used for the determination of biomarkers.

Transformation of multivariate data into a different feature space using a kernel function called the 'radial basis function', allowed linear separation of data by SVM. SVM parameters were optimized by venetian blinds (10 data splits) cross-validation. Model validation was performed with 30% of the samples' spectra randomly selected as an external test set. Success of this was measured by evaluation of specificity, sensitivity, and accuracy.

To explore the relationship of controlled environmental variables with plant spectral profiles, each treatment category was scored either a zero (low) or a one (high) in each of the supplied variables of nitrogen, micronutrients, water, and R: FR, see Supplementary Table S3. This binary dataset was compared with ATR-FTIR spectral absorbances using a multivariate analysis technique called PLSR. The resultant regressions gave an indication of which independent variable had the greatest impact on spectral absorbances. PLSR was performed using PLS Toolbox version 7.9.3 (Eigenvector Research, Inc., Manson, USA). Multivariate analysis techniques allow multiple variables to be compared at the same time, enabling spectral absorbance values across a range of wavelengths to be simultaneously correlated against environmental or physiological variables of numerous samples. Observing all these data at once allows patterns to be seen and enables predictions to be made.

PLSR was additionally used to predict plant physiological conditions, such as Ψ_{root}, by comparison of ATR-FTIR spectral data and measured water potential data. To form these models, an X-block of ATR-FTIR spectral absorbance data for plants was analysed by PLSR against a Y-block of physiological variables for the corresponding plants. Environments were analysed separately, allowing a model to be created for each of them. Once made, these models can be applied to new ATR-FTIR spectral data in the absence of measured physiological variables such as root water potential, to non-destructively predict these variables.

Results

Knotweed plants exhibit environmentally induced phenotypes.

The response of Japanese knotweed to the environmental treatment conditions (LC, LD, LN, LLN, SC, SD, SN, SLN) was sufficient to induce measurable physiological differences. Leaf area was significantly lower for LD (510 cm^2) than LC (1028 cm^2), see Fig. 1a. In general, shaded
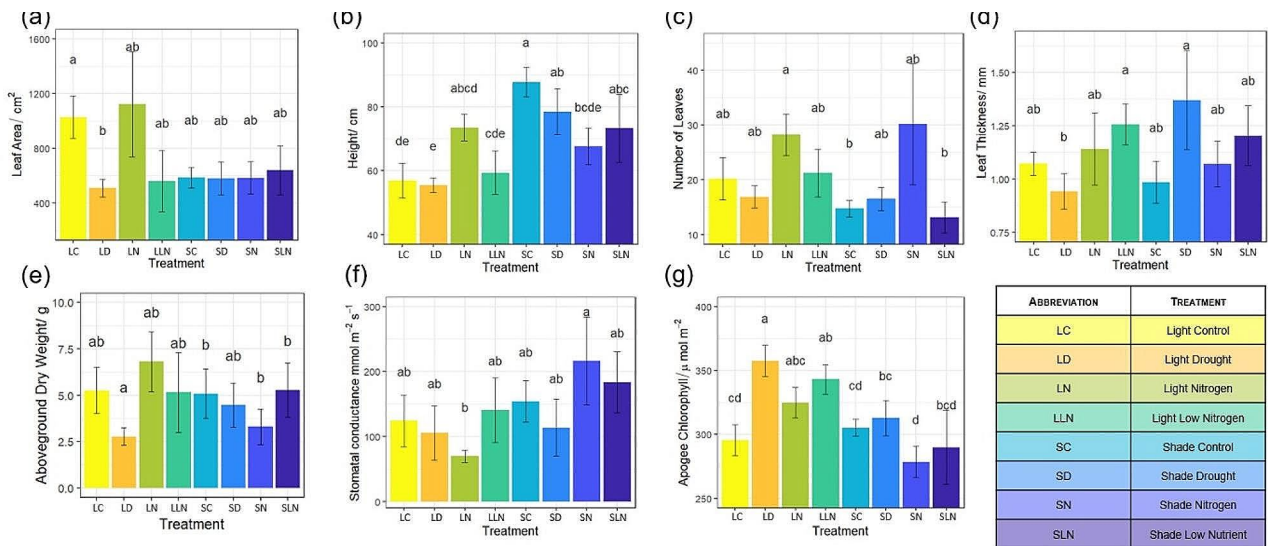
Fig. 1 Effects of each treatment on the physiological parameters **(a)** leaf area **(b)** height **(c)** number of leaves **(d)** leaf thickness **(e)** aboveground dry weight **(f)** stomatal conductance **(g)** Apogee chlorophyll, grouped by treatment

Fig. 2 Effects of the growth environment on plant water relations: **(a)** leaf and **(b)** root water potential measured in MPa
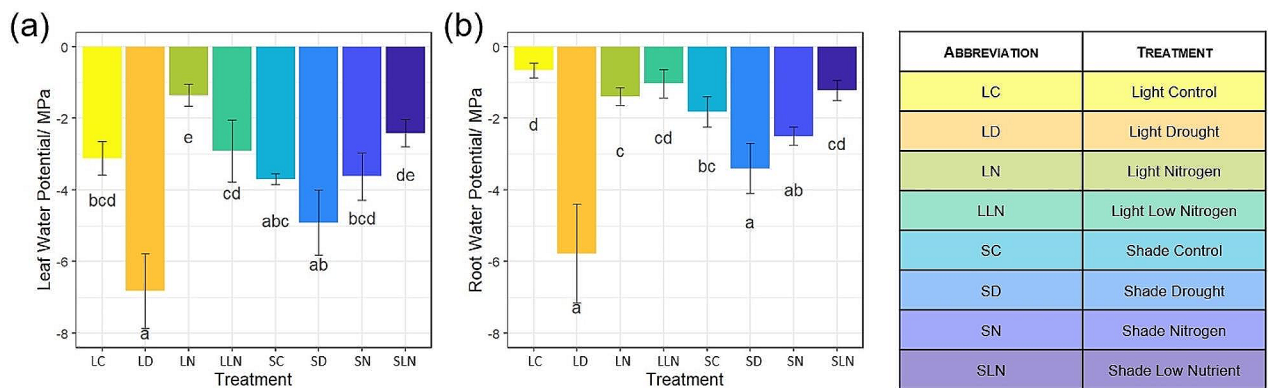
plants (SC, SD, SN, and SLN) were taller and etiolated, averaging 76.8 cm in height, compared with those of the light cabinet (LC, LD, LN and LLN), which averaged 61.3 cm (Fig. 1b). However, plants supplemented with nitrogen only (LN and SN) were different to the general trend for each light treatment. SC and SLN plants had fewest leaves, ~15 and ~13 leaves respectively, whilst LN had the most, ~30, leaves (Fig. 1c). Leaf thickness was higher SD and LLN than LD (Fig. 1d). Of the plants with a high R: FR (LC, LD, LN and LLN) the aboveground dry weight was lowest under drought conditions (LD; Fig. 1e). This differed from shaded plants (SC, SD, SN and SLN) in which SN had the lowest aboveground dry weight (Fig. 1e). Aboveground fresh weight was lower in LD than SC, SN and SLN (Supplementary Figure S3a). Stomatal conductance in SN plants was three times that of LN (Fig. 1f). Chlorophyll was highest in LD, LLN and LN (358, 343 and 325 µmol.m^{-2}), followed by SD, SC, LC

and SLN (313, 305, 296, 290 µmol.m^{-2}), and the lowest levels were measured in SN (278 µmol.m^{-2}, Fig. 1g).

Statistical significance was calculated using a Kruskal-Wallis followed by a post hoc test using the criterium Fisher's least significant difference (LSD) to determine where the difference lies, signified by lowercase letters above the bars. Within each graph, all bars which share letters are not significantly different from each other. Data are mean +/- standard errors. N values for groups LC, LD, LN, LLN, SC, SD, SN, and SLN respectively: Leaf area 5, 5, 5, 4, 3, 6, 5, 6; height 10, 9, 8, 8, 8, 6, 7, 8, number of leaves 10, 9, 8, 8, 8, 6, 7, 8; leaf thickness 7, 5, 7, 7, 5, 3, 5, 6; aboveground dry weight 6, 8, 7, 5, 4, 6, 6, 7; stomatal conductance 5, 7, 4, 4, 6, 4, 4, 4; and chlorophyll 7, 7, 7, 8, 5, 6, 6, 7 (four technical replicates).

Plant water status, evidenced by Ψ_{leaf} and Ψ_{root}, was also affected markedly by treatments (Fig. 2a-b). LD, SD, and SC plants had the most negative Ψ_{leaf}, (-6.8, -4.9

and −3.7 MPa respectively) indicating lowest hydration, followed by SN, LLN and LC (-3.6, -2.9, and −3.1 MPa respectively), whilst SLN and LN had the least negative leaf water pressures (-2.4 and −1.4 MPa respectively) indicating the highest levels of hydration (Fig. 2a). LD, SD, and SN had the most negative root water potentials (-5.8, -3.4 and −2.5 MPa respectively) indicating lowest hydration, followed by SC (-1.8 MPa), then LN, LLN, SLN (-1.4, -1.0 and −1.2 MPa), and LC (-0.7 MPa) had the Ψ_{root} nearest to zero indicating the best levels of hydration (Fig. 2b).

Statistical significance was calculated using a Kruskal-Wallis followed by a post hoc test using the criterium Fisher's least significant difference (LSD) to determine where the difference lies, signified by lowercase letters above the bars. Within each graph, all bars that share letters are not significantly different from one another. Data are mean +/- standard errors. Leaf water potential $n=6$, 8, 7, 6, 4, 6, 5, 7 and root water potential $n=6$, 8, 5, 6, 4, 5, 4, 5 for groups LC, LD, LN, LLN, SC, SD, SN, and SLN respectively.

Physiological changes are reflected in the ATR-FTIR spectra of plants.

The response of Japanese knotweed leaves to the environmental treatment conditions (LC, LD, LN, LLN, SC, SD, SN, SLN) was observed in marked differences in their spectral profiles. Figure 3a shows the class mean fingerprint spectra for the different environmental conditions, with the strongest absorbance peaks at approximately 1750, 1650 and 1030 cm^{-1}. Although further chemometric analysis is required to gain more information, Fig. 3b demonstrated visual differences between pre-processed spectra taken from plants in different treatment categories. Where the spectral profiles do not overlap, such as the horizontal shifts at ~ 1400 and ~ 1550 cm^{-1}, and the vertical divergences at ~ 1600 and 1750 cm^{-1}, this is indicative of biomolecular differences in concentration and chemical structure respectively.

To further explore the response of Japanese knotweed to the applied environments, chemometric techniques were applied to the acquired spectra. PCA alone did not achieve separation between treatment groups, with clusters overlapping (Fig. 4a). The symmetrical pattern in Fig. 4a was reflective of the two leaf surfaces, with separation of each in a different direction along the PC1 scores axis. This was confirmed by principal component analysis of the spectral data from all treatment categories grouped by leaf surface; Supplementary Figure S2 shows lower surface spectra grouped on the left and upper surface spectra grouped on the right. Following the application of PCA-LDA to dried-leaf spectra, the different treatment types are separated into clusters along the axis LD1 (Fig. 4b), in particular the separation between shaded and light grown samples. SVM of whole dried leaves (cost=31.6228, γ = 3.1623, N_{SV}: 400) achieved excellent separation between categories (see Fig. 4c-d), attaining the performance measures of 94.9% accuracy, 91.0% sensitivity, and 98.8% specificity.

Note that the PC1 axis in a) separates the spectra taken from the lower leaf surface to the left of zero and those from the upper surface are on the right, see Supplementary Figure S2.

Plant responses to environment are associated with specific environmental response biomarkers.

Molecular differences between plants of the eight treatments were examined using PCA-LDA (Fig. 4b). The top eight PCA loadings (Supplementary Figures S4-S15), which represent the main qualitative wavenumbers discriminating each treatment comparison, were subsequently selected for the identification of biomarkers to qualitatively characterise the biochemical compounds showing the greatest changes, see Table 1. Many of the assigned biomarkers are cell wall carbohydrates and the proteins which regulate them, as well as molecules which other studies have identified as indicators of abiotic stress.
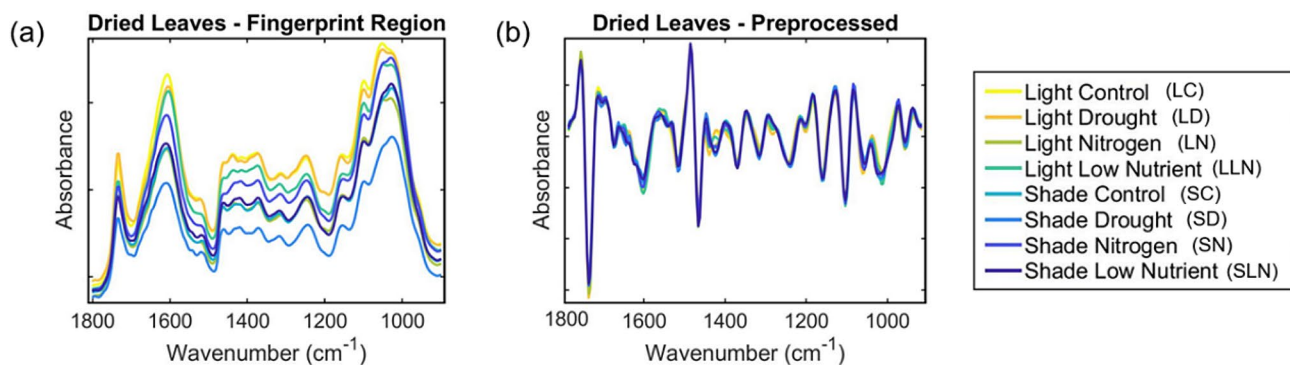
Fig. 3 (a) Class means fingerprint region (1800–900 cm^{-1}) and (b) pre-processed (SG second differentiation $n=9$ and vector normalisation) class means spectra in the fingerprint region (1800–900 cm^{-1}) from dried leaves, grouped by treatment
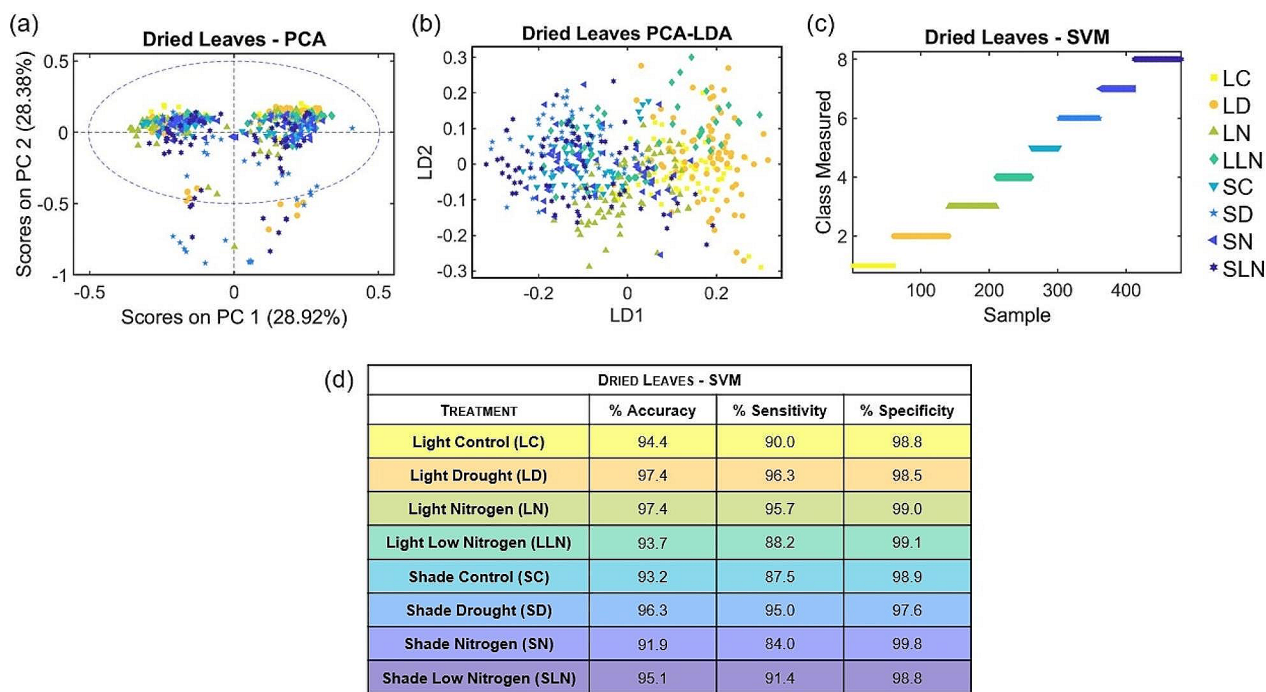
Fig. 4 **(a)** PCA scores plot, **(b)** PCA-LDA scatter plot, **(c)** SVM sample/measured plot and **(d)** SVM results for spectra taken of dried leaves grouped by treatment

PLS regression allows predictions of physiological responses.

Plant environmental responses to different treatment groups were reflected in the differences in both physiological measurements (Figs. 1 and 2) and in the acquired ATR-FTIR spectral profiles (Fig. 3). Two such datasets can be combined to correlate spectral profiles with phenotypic responses [77]. Similarly, the phenotypic changes measured here can form training and test data for models which demonstrate the potential of mid-infrared (MIR) spectroscopy for the rapid, non-destructive prediction of plant physiology. Figure 2 shows that Ψ_{leaf} and Ψ_{root} were affected markedly by treatments (Fig. 2a-b). The largest Ψ_{root} was found in LD (-5.8 MPa) compared with LC (-0.7 MPa) which had the smallest. Therefore, these two categories were chosen to develop a model for the prediction of plant water status. Figure 5 is an exemplar PLS regression graph for the prediction of physiological parameters using ATR-FTIR spectral data. This shows the PLS regression of Ψ_{root}, as measured with a pressure chamber (Model 3000F01 Plant Water Status Console, Soil Moisture Equipment Corp., Santa Barbara, CA, USA), against predicted levels using ATR-FTIR spectral absorbances of intact dried leaves grown under LC and LD conditions as training data, showing an example of the predictive models generated using this approach. The green line in Fig. 5 shows the ideal prediction gradient of one, which would be 100% accurate, and the red

line shows the achieved success of the model, which was a gradient of $R^2 = 0.8$ indicating a successful prediction. The key wavenumbers for this PLSR prediction of Ψ_{root} are shown in a loadings graph (Supplementary Figure S17), which provide useful spectral indicators of drought. This further highlights the power of such models when investigating the responses of plants to environmental variables and the impacts these have on growth and development, particularly in species which are recalcitrant to the destructive and time-consuming physical techniques routinely used for such measurement.

Yellow squares indicate data points from LC plants and orange circles represent data from LD plants. The green line shows the ideal prediction gradient of one, which would be 100% accurate. The red line shows the achieved success of the model. Model parameters are as follows: RMSEC: 1.4966, RMSECV: 1.6844, Calibration Bias: 3.1086e-15, CV Bias: -0.009925, R^2 Cal: 0.841332, R^2 CV: 0.799426.

Light environment R: FR ratio has the greatest impact on the plant spectral profiles.

Insights into which independent variable had the greatest impact on spectral absorbances were gained through PLS regression of the binary dataset in Supplementary Table S3 against spectral absorbances. Table 2 shows the results of this PLS regression, with higher R^2 values indicating a greater contribution from the corresponding abiotic variable. The red: far-red ratio had the greatest

Table 1 Loadings and biomarkers for discrimination between spectral profiles of plants from different treatment categories

	Molecular Assignment	Wavenumbers (cm^{-1})	Reference	Comparison											
				LC vs. LD	LC vs. LN	LC vs. LLN	LC vs. SC	LD vs. SD	LN vs. LLN	LN vs. SN	LLN vs. SLN	SC vs. SD	SC vs. SN	SC vs. SLN	SN vs. SLN
Carbohydrates	C=O stretching vibration of alkyl ester in pectin	1748, 1612	[67, 68]	✓									✓	✓	
	Ring vibration of pectin	1319	[67]			✓								✓	
	OCH$_3$ (polysaccharides, pectin)	972	[69]							✓					
	Starch	1042, 1030, 1026, 1022	[70]	✓	✓		✓			✓		✓			
	β-glucans	1427	[71]	✓	✓		✓								
	Stretching vibrations [ν(CO)] of the COC glycosidic linkage of polysaccharides	1130	[71]			✓							✓		
	Bending vibration δ(CH) polysaccharides	1443	[66]									✓	✓		
	C–O & C–C stretching; (C–O–H) bending of cellulose (abaxial surface)	1049	[72]					✓						✓	
	Hemicellulose	1732	[73]	✓			✓	✓							
	ν(C–O) and ν(C–C), disaccharides, sucrose	1126	[69]		✓										
	C=O stretching of carbonyl group, typical saccharide absorption	1636	[69]			✓		✓							
	C–O–C bending vibration (fructo-oligosaccharides)	1134	[74]						✓						
	C–C stretching ring (galactan and rhamnogalacturonan)	1072	[71]						✓						
	ν(CC) skeletal cis conformation, ν(CH$_2$OH); Galactan ν(CO) stretching coupled with C–O bending;	1038	[73]							✓	✓				✓
Bases	C=O thymine	1713	[69]	✓		✓						✓			
	C=N adenine	1609, 1574	[69]	✓											✓
	Modified guanine	1531	[69]	✓	✓										
	RNA stretching, ring bending of uracil	988	[69]												
	C–O stretching of the phosphodiester and the ribose	991, 1065	[69]			✓					✓				
	C–N–C stretch of nucleic acids	968	[69]							✓					
	nucleic acids due to the base carbonyl (C=O) stretching and ring breathing mode	1690	[69]							✓					
Proteins	Phosphate I (stretching PO$_2^-$ symmetric vibration) in B-form DNA	1088	[69]	✓						✓		✓			
	Ring base	1566	[69]	✓											✓
	Protein	1709	[45]	✓	✓		✓								
	Protein phosphorylation	953	[73]	✓	✓		✓								
	Amide I	1670, 1647, 1651, 1639, 1628, 1585	[69, 75]	✓	✓	✓	✓			✓	✓	✓	✓	✓	✓
	Amide II: (protein N–H bending, C–N stretching), α-helical structure	1570, 1547	[69]								✓	✓			
	Amide III	1323	[66]							✓					
	Symmetric CH$_3$ bending of the methyl groups of proteins	1396	[69]					✓							
	Tyrosine	1512	[69]									✓			

Table 1 (continued)

Molecular Assignment	Wavenumbers (cm⁻¹)	Reference	LC vs. LD	LC vs. LN	LC vs. LLN	LC vs. SC	LD vs. SD	LN vs. SN	LLN vs. SLN	SC vs. SD	SC vs. SN	SC vs. SLN	SN vs. SLN
Lipids													
CH₃ bending of proteins and lipids	1393	[75]		✓	✓	✓							
Lipid; fatty acid esters	1732	[73]				✓	✓				✓		
CH₂ bending in lipids	1466, 1470	[45, 69]				✓	✓			✓	✓		
Ester C=O stretch: triglycerides, cholesterol esters	1744	[69]						✓					✓
Ester C=O stretching vibration (phospholipids)	1740	[69]										✓	
Other													
Pentanone	1385, 1157, 957	[76]	✓	✓		✓							
Ring C–C stretch of phenyl	1589, 1582	[69]			✓				✓				
In-plane C–O stretching vibration combined with the ring stretch of phenyl	1339	[69]							✓				
Ring stretching (C–C)–d(C–H)	999	[66]					✓						
C=O band	1728	[69]						✓					
Asymmetric phosphate; ν(C–O–C) of geranyl acetate (acyclic monoterpene)	1227	[73]						✓	✓				
PO₂⁻ asymmetric stretching (Phosphate I)	1265, 1242, 1211, 1207	[69]								✓	✓		
CHα rocking	1265	[69]								✓			
Symmetric phosphate stretching	1092	[75]									✓	✓	
Stretching vibrations of hydrogen-bonding C–OH groups	1161	[69]											✓

influence over the spectral profile of intact dried leaves, reaching the highest R^2 of 0.3, whilst water, micronutrients, and nitrogen all contributed R^2 values of 0.1. The RMSECV, representing the error in the predicted environmental parameter, was higher for prediction of micronutrient conditions at 0.5, than the other parameters at 0.4.

Discussion

Environmental response can be detected through leaf spectral profiles.

The measured physiological parameter in Figs. 1 and 2 show clearly that the genetically identical plants responded to the applied treatment conditions with environmentally induced phenotypes, demonstrating the plasticity expected of this species [28–35]. The acquired ATR-FTIR spectral absorbances in Fig. 3 demonstrate that the environmental conditions under which plants are grown have a marked impact on their spectral profiles suggesting subtle changes in plant composition. Although the overall absorbance pattern of the fingerprint region in Fig. 3a is visually similar to that of any other green vegetative plant tissue [48, 78, 79], chemometrics has the power to extract more information, including differences between treatment groups. The unique patterns produced by the ATR-FTIR spectral absorbance profiles of plants grown in different environments could be successfully differentiated through application of the discriminant algorithm, SVM (Fig. 4c-d). This combined method achieved high accuracy, sensitivity, and specificity. This is consistent with observations from previous studies which have identified spectra from plants of different growing environments [48–53] suggesting that the high degree of plasticity exhibited by Japanese knotweed to environmental factors is reflected in key biomolecular changes that may contribute to its success as an invasive species.

Detected biomarkers are associated with plant stress responses.

A variety of biological compounds, such as proteins, ketones, terpenes, and carbohydrates, which differ under each condition were identified through linking molecular biomarkers with key wavenumbers affected by environment. The peak at 1709 cm⁻¹ (Figures S4 and S7), which was assigned to protein absorbance (see Table 1), is a common biomarker across other plant species, and has been associated with plant development in tomato plants [75]. This band indicates the relative concentrations of the significant proteins are highest in LD, followed by LC, and lowest in LN. The upregulation of these proteins under conditions of drought stress and increased micronutrient availability suggests that the peak at 1709 cm⁻¹ may correspond to enzymes that break down polysaccharides in plant cell walls, such as pectin-methylesterase and β-glucosidase. These enzymes

Fig. 5 Prediction of root water potential (Ψ_{root}) from ATR-FTIR spectral data in the fingerprint region (1800–900 cm^{-1}) of plants from categories LC and LD using PLS regression

Table 2 Model parameters of PLSR correlation of intact leaf spectral profiles with controlled environments assigned binary values

Model parameters	Nitrogen	Micronutrients	Red: far-red ratio	Water
R^2	0.1	0.1	0.3	0.1
RMSECV	0.4	0.5	0.4	0.4

allow for leaf expansion during development and stress-induced alterations of cell-wall polymers [80]. Another response of Japanese knotweed plants to water deficit is highlighted by biomarker 1385 cm^{-1} which was assigned to the bioactive plant volatile, pentanone. Spectral comparison suggests that pentanone was higher in control plants (LC) than droughted plants (LD). This is consistent with a similar spectroscopic study on citrus plants in which pentanone was retained in healthy leaves but released under biotic stress [76]. It seems possible that this finding could be related to the hormone jasmonic acid, which contains a pentanone ring. This hypothesis is supported by hormonal data in which jasmonic acid levels were higher in LC than in plants grown under less ideal conditions [77]. The jasmonic acid signalling pathway is a core component in plant response to both biotic and abiotic stress [81]. The peak at 953 cm^{-1}, caused by protein phosphorylation, was a key difference in several comparisons; LC vs. LD, LLN vs. SLN, SC vs. SN, and SC vs. SLN. This indicates that wavenumber-953 is sensitive to changes induced by drought, and the combination of

stresses from a low R: FR and deficiencies in nitrogen and micronutrients. Similarly, the peak at 1732 cm^{-1}, associated with hemicellulose [73], was a key difference between LC vs. SC, LD vs. SD, and SC vs. SN, whilst 1038 cm^{-1}, associated with the polysaccharide galactan [73], allowed discrimination between LLN vs. SLN and SN vs. SLN. The association of these peaks with abiotic stress is consistent with other spectroscopic studies which have associated them with vehicular pollution in sycamore trees [73]. Wavenumber 1227 cm^{-1}, assigned to geranyl acetate, an acyclic monoterpene, was higher in LLN than SLN. This biomarker has previously been associated with response to ozone exposure in sycamore tree leaf tissue [73]. Amide I peaks at 1628 and 1585 cm^{-1}, have previously been associated with fungal infection in other studies [73]. In the present study, these two Amide I peaks were key differences between plants not provided with any nutrients and those provided with nitrogen only. It is common for plant responses to biotic and abiotic stresses to overlap because stress signalling pathways are known to share intermediates such as reactive oxygen species and calcium which allow for crosstalk [82]. Taken together these results suggest that wavenumbers 953, 1038, 1227, 1709, and 1732 cm^{-1} are key indicators of plant-environment interactions, including abiotic stress responses, that are conserved between species.

When the ATR-FTIR spectral profiles of plants grown under different environments were compared, several cell wall carbohydrates, both structural and storage, were highlighted as significantly different. The storage

molecule starch, reserves of which are known to be mobilised under conditions of abiotic stress [81], was identified as a biomarker for five of the comparisons [70]. As outlined above, the peak for hemicellulose (1732 cm^{-1}) was a key difference between shaded and unshaded plants both under, and in the absence of, drought stress [73]. Shading stress is known to have a greater inhibitory effect on the biosynthesis of non-structural than that of structural carbohydrates [83]. Some structural carbohydrates, such as xylose and mannose, decrease under shading stress [83]. Beta- glucans were highlighted as a key differentiator between plants grown with differing red: far-red ratios, LC and SC again showing hemicellulose to be affected by shading. Also differentiated by this beta- glucan peak were LC and LN, indicating a consequence of environmental micronutrient levels. Wavenumber 1126 cm^{-1} identified sucrose, the major transport form of photo-assimilated carbon, as a key discriminator between LC and LN, but not their shaded equivalents SC and SN [69, 84]. The peak at 1049 cm^{-1} for cellulose [72] was a key discriminator between SC and SLN, showing the impact of nutrient deficiency on plants also experiencing shading. Low levels of soluble sugar, sucrose, lignin and cellulose content can result in weak stem strength [83]. However, this was not reflected in the measured stem diameter of plants, variations in which were insignificant across all eight treatments (see Supplementary Figure S3a). Etiolation was observed in shaded plants from SC, SD and SLN which were significantly taller than those of the non-shaded groups LC, LD and LLN (see Fig. 1b). One molecule which can alter elongation capacity of the cell wall is galactan (see peaks 1072 and 1038 cm^{-1}). It achieves this by controlling porosity and viscoelastic properties of the cell wall [85] and levels increase during the cell expansion phase [86]. Galactans also play a role as cell wall storage polysaccharide [86]. The amplitude of peaks 1072 and 1038 in the rubber band normalised fingerprint spectra indicate that galactan was present in higher concentrations in LN than LLN, SN than SLN, and in LLN than SLN, but this peak was not identified as a key difference for other comparisons. These results suggest that Japanese knotweed plants which are experiencing shading and deficiency of both micronutrients and nitrogen have lower levels of galactan, because they have low requirements for carbohydrate storage and lack the excess resources for expansion and growth.

'Tarping', an herbicide-free control strategy where soil covered with a plastic tarp is heated by solar radiation and thought to reach a lethal temperature for knotweed growth [87], is more effective when black, light-blocking tarp is used [88]. The combined stresses of shade and low nutrients observed in this study suggests that the additional shading effect of tarping would be most effective in areas of poor soil quality or those prone to leaching.

Artificial shading may also increase the efficacy of herbicides that function through interference with nutrient absorption and metabolism.

The red: far-red ratio had the greatest effect on leaf spectral profiles.

Differences in spectral profiles indicate key biomolecular alterations occurring within the leaves under different growth environments, reflective of the high degree of environmental plasticity exhibited by Japanese knotweed that may contribute to its success as an invasive species [89, 90]. Although IAS generally display greater plasticity, this is not always correlated with a fitness benefit [91]. Physiological variation of Japanese knotweed grown in different habitats has been recorded in previous studies, including differences in height, number of leaves, leaf surface area and biomass allocation [92, 93]. All the rhizomes used for these controlled growth experiments were extracted from the same source, but recent research indicates that the environmental adaptations observed here may be influenced by the original source of the rhizomes and could have differed if these were collected from another habitat type [93]. The growth environment plays a significant role in phenotypic presentation, and this study has explored the influence of specific environmental variables.

Chlorophyll content under drought stress can both increase [94] and decrease [95]. Here, LD had significantly higher chlorophyll levels compared with LC (Fig. 1g). This may be because LD had fewer (Fig. 1c), smaller (Fig. 1a), leaves compared with LC, leading to a necessity for increased chlorophyll levels per unit leaf area. Figure 1 shows that plants of the nitrogen supplemented category, SN, had a significantly greater number of leaves than SC or SLN, but this was not statistically different to SD. Although drought is usually associated with a reduced leaf number [96, 97], this observation is consistent with water having only been withheld completely for seven days out of a total growth period of fifty days in the present study, representing a short-term drought rather than a long term water deficit. However, nitrogen availability, sugar demand, R:FR and auxin concentrations have all been linked to the control of apical branching [98–100]. These pathways interlink via common intermediates, for example a low R: FR promotes auxin signalling [100] and nitrogen fluctuations have a significant impact on auxin distribution [98]. These complex interacting signals could explain the lack of significant differences in the number of leaves between categories. Growth was markedly affected in shaded plants (LC, LD, LN and LLN) which were generally taller in height (Fig. 1). This is consistent with ethylene-mediated stem elongation which is a stress response known to be induced by low R: FR [101]. Additionally, transpiration rate is elevated under high R: FR [102] thereby increasing the likelihood of

Holden *et al. BMC Plant Biology*   (2024) 24:769

Page 12 of 16

plants experiencing drought under conditions of reduced water availability, possibly leading to the larger root water potentials measured in category LD compared to category SD. This increased transpiration rate may also have altered the effect of drought on leaf quantity under different lightings; under a high R: FR LC plants had more leaves than LD, however under a low R: FR then SD had more leaves than SC, see Fig. 1.

Of the altered environmental parameters, the R: FR of the growth environment had the greatest effect on the spectral profiles of intact dried leaf material. This was indicated by the highest PLS regression R^2 in Table 2. A possible explanation for this is that these spectra were taken from leaf vegetative tissue, which may be more prone to changes in light as leaves are photosynthetic organs. The primary function of leaves is to absorb sunlight for photosynthesis, and spectra of other plant organs may be affected differently by different environmental factors. The clustering pattern of the 2D PCA-LDA scatter graph (Fig. 4b) provides an indication of why the R: FR has the greatest impact on the spectra. This displays a general separation along the axis LD1 of shaded samples on the left and non-shaded samples on the right. This LD1 axis is significant for identifying the wavenumbers most affected by the different environments, used for the classification of groups. Molecular biomarkers were found from the LD1 loadings and indicate which molecules differ most between leaves of plants grown in different environments: lipid (1732 cm^{-1}), CH_2 bending of the methylene chains in lipids (1470 cm^{-1}), ring breathing (995 cm^{-1}), C-H and O-H bending in hemicellulose (1423 cm^{-1}), C-O vibration in sucrose (1126 cm^{-1}), overlapping of the protein amide III and the nucleic acid asymmetric phosphate vibration (1231 cm^{-1}), cellulose (1319 cm^{-1}), peak of nucleic acids due to the base carbonyl stretching and ring breathing mode (1620 cm^{-1}), starch (1030 cm^{-1}), and CH_3 rocking (957 cm^{-1}) [67, 68, 101–104].

The sensitivity of ATR-FTIR spectral profiles to the R: FR ratio of the growth environment could account for some of the spectral differences in plants grown in different regions of the UK, observed previously [48]. At higher latitudes, plants experience longer durations of sunlight from low solar angles [105]. The R: FR ratio at low solar angles is lower [106] and more variable [105]. Water vapour increases the R: FR photon ratio by preferentially absorbing the FR light meaning that plants in growing regions with overcast skies tend to experience a higher R: FR ratio than those under clear skies [107]. Additionally, modelled climate scenarios predict that increasing global temperatures will result in increased atmospheric water vapour, which will reduce the proportion of far-red photons in sunlight [106]. Plants sense the R: FR ratio with phytochromes which allows them

to trigger their shade-avoidance response and detect above-ground neighbours [108]. As a pioneer species, one could predict Japanese knotweed to be a competitive shade-avoider, likely to have a strong avoidance response compared with a shade-tolerant woodland floor species, however, leaves within the dense knotweed canopy are known to experience reduced light-penetration. Martin FM et al. [109] noted the lack of information on the significance of shading for Japanese knotweed, particularly in interaction with mechanical control, whilst observing its importance for ramet density (the space between independent members of a clone). Plants grown in shaded conditions (SC, SD, SN, SLN) tend to have lower aboveground fresh and dry weights compared with light (LC, LD, LN, LLN), see Fig. 1 and Supplementary Figure S2, supporting the importance of light quality for Japanese knotweed. These results have been echoed in field studies which found that a reduction in soil fertility had no significant effect on knotweed biomass production, and concluded that light quality was the most important of the tested parameters [110].

ATR-FTIR spectroscopy provides a novel tool for predicting physiological responses.

The model in Fig. 5 was created using training data from plants of LC and LD, which differed only in the amount of water supplied to them with the other controlled environmental variables remaining the same. The use of larger training sets would allow the generation of more robust models which take account of the breadth of the variables in the growth environment enabling this approach to be widely applied. We have previously shown the power of ATR-FTIR spectroscopy for predicting plant physiological responses such as hormone concentrations [77]. Applying this approach to the analysis of plant water status in Fig. 5 further highlights the importance of such predictive models for non-destructively studying the responses of plants to their environment in situ. Near-infrared (NIR) spectroscopy [111] using portable hand-held NIR spectrometers, whilst less rich in the spectral information provided compared with ATR-FTIR spectroscopy, has been used for monitoring plant water [112–114] and nutrient [115] status. Advances in technology mean that portable MIR spectrometers are now available [116–120] highlighting the potential of this method for future applications of MIR spectroscopy to the prediction of physiological responses in the field, providing a more sensitive alternative to NIR spectroscopy. The use of MIR as an indicative tool to determine the efficacy of treatment approaches for invasive knotweeds could accelerate studies which normally span several years [121], and provide dosage guidance for herbicide application to prevent sub-lethal outcomes. ATR-FTIR spectral ground-readings could complement spatial dynamic data collected by remote sensing [122], to create detailed predictive maps

that enhance our ability to monitor invasive alien species, providing further information on the 'what' in addition to the 'where'.

Conclusions

This study indicated that the R: FR ratio of the light environment, plays a key role in shaping the spectral profile of Japanese knotweed. Spectral differences between plants of different treatment groups allowed the identification of several biomarkers for environmental effects, highlighting changes in compounds such as cell wall carbohydrates. Conservation of specific wavenumbers across plant species raises the potential for their use as indicators of plant health under abiotic stress.

Supplementary Information

The online version contains supplementary material available at https://doi.org/10.1186/s12870-024-05200-7.

Supplementary Material 1

Data availability
The datasets generated and analysed during the current study are available in a supplementary folder.

Declarations

Ethics approval and consent to participate
Permission was granted from local landowners for collection of rhizomes for use in this study. All experimental studies on plants were complied with relevant institutional, national, and international guidelines and legislation.

Consent for publication
Not applicable.

Competing interests
Martin Robert McAinsh of Lancaster University is an editor for BMC Plant Biology. All other authors declare no competing interest.

Author details
[1]Lancaster Environment Centre, Lancaster University, Lancaster LA1 4YQ, UK
[2]Phlorum Ltd, Brighton BN2 6AH, UK
[3]Biocel Ltd, Hull HU10 7TS, UK
[4]Department of Cellular Pathology, Blackpool Teaching Hospitals NHS Foundation Trust, Whinney Heys Road, Blackpool FY3 8NR, UK

1.7 References
1. Diez JM, D'Antonio CM, Dukes JS, Grosholz ED, Olden JD, Sorte CJB, et al. Will extreme climatic events facilitate biological invasions? Front Ecol Environ. 2012;10:249–57.
2. Parepa M, Fischer M, Bossdorf O. Environmental variability promotes plant invasion. Nat Commun. 2013;4:1–4.
3. Bellard C, Jeschke JM, Leroy B, Mace GM. Insights from modeling studies on how climate change affects invasive alien species geography. Ecol Evol. 2018;8:5688–700.
4. Head L. The social dimensions of invasive plants. Nat Plants. 2017;3:1–7.
5. Chinchio E, Crotta M, Romeo C, Drewe JA, Guitian J, Ferrari N. Invasive alien species and disease risk: an open challenge in public and animal health. PLoS Pathog. 2020;16:e1008922.
6. Pyšek P, Hulme PE, Simberloff D, Bacher S, Blackburn TM, Carlton JT, et al. Scientists' warning on invasive alien species. Biol Rev. 2020;95:1511–34.
7. Pejchar L, Mooney HA. Invasive species, ecosystem services and human well-being. Trends Ecol Evol. 2009;24:497–504.
8. Bradshaw CJA, Leroy B, Bellard C, Roiz D, Albert C, Fournier A, et al. Massive yet grossly underestimated global costs of invasive insects. Nat Commun. 2016;7:1–8.
9. Shackleton RT, Shackleton CM, Kull CA. The role of invasive alien species in shaping local livelihoods and human well-being: a review. J Environ Manage. 2019;229:145–57.
10. Morris TL, Esler KJ, Barger NN, Jacobs SM, Cramer MD. Ecophysiological traits associated with the competitive ability of invasive Australian acacias. Divers Distrib. 2011;17:898–910.
11. Davis MA, Grime JP, Thompson K. Fluctuating resources in plant communities: a general theory of invasibility. J Ecol. 2000;88:528–34.
12. Nicotra AB, Atkin OK, Bonser SP, Davidson AM, Finnegan EJ, Mathesius U, et al. Plant phenotypic plasticity in a changing climate. Trends Plant Sci. 2010;15:684–92.
13. Fowler D, Coyle M, Skiba U, Sutton MA, Cape JN, Reis S et al. The global nitrogen cycle in the twenty-first century. Philosophical Trans Royal Soc B: Biol Sci. 2013;368.
14. Valliere JM, Escobedo EB, Bucciarelli GM, Sharifi MR, Rundel PW. Invasive annuals respond more negatively to drought than native species. New Phytol. 2019;223:1647–56.
15. Williams, Frances & Eschen, René & Harris, Anna & Djeddour, Djami & Pratt, Corin &Shaw, Richard & Varia, Sonal & Godwin, Julien & Thomas, Sarah & Murphy, Sean. (2010).The Economic Cost of Invasive Non-Native Species on Great Britain.
16. Parepa M, Kahmen A, Werner RA, Fischer M, Bossdorf O. Invasive knotweed has greater nitrogen-use efficiency than native plants: evidence from a 15 N pulse-chasing experiment. Oecologia. 2019;191:389–96.
17. Wilson SD, Tilman D. Components of plant competition along an experimental gradient of nitrogen availability. Ecology. 1991;72:1050–65.
18. Broadbent A, Stevens CJ, Peltzer DA, Ostle NJ, Orwin KH. Belowground competition drives invasive plant impact on native species regardless of nitrogen availability. Oecologia. 2018;186:577–87.
19. Science and Technology Committee - House of Commons. Japanese knotweed and the built environment. Sci Technol Comm Rep. 2019;:13.
20. Rouifed S, Byczek C, Laffray D, Piola F. Invasive knotweeds are highly tolerant to salt stress. Environ Manage. 2012;50:1027–34.
21. Michalet S, Rouifed S, Pellassa-Simon T, Fusade-Boyer M, Meiffren G, Nazaret S, et al. Tolerance of Japanese knotweed s.l. to soil artificial polymetallic pollution: early metabolic responses and performance during vegetative multiplication. Environ Sci Pollut Res. 2017;24:20897–907.
22. Sołtysiak J. Heavy metals tolerance in an invasive weed (fallopia japonica) under different levels of soils contamination. J Ecol Eng. 2020;21:81–91.
23. Zhang Y-Y, Parepa M, Fischer M, Bossdorf O. Epigenetics of colonizing species? A study of Japanese knotweed in Central Europe. In: Barrett SCH, Colautti RI, Dlugosch KM, Rieseberg LH, editors. Invasion Genetics. Chichester, UK: John Wiley & Sons, Ltd; 2016. pp. 328–40.

24. Richards CL, Schrey AW, Pigliucci M. Invasion of diverse habitats by few Japanese knotweed genotypes is correlated with epigenetic differentiation. Ecol Lett. 2012;15:1016–25.

25. Holm AK, Elameen A, Oliver BW, Brandsæter LO, Fløistad IS, Brurberg MB. Low genetic variation of invasive Fallopia spp. in their northernmost European distribution range. Ecol Evol. 2018;8:755–64.

26. Hollingsworth ML, Bailey JP. Evidence for massive clonal growth in the invasive weed Fallopia japonica (Japanese knotweed). BokanicalJouml Ofrhc Linn So&&. 2000;133:463–72.

27. Bailey JP, Conolly AP. Prize-winners to pariahs -A history of Japanese Knotweed s.l. (Polygonaceae) in the British Isles. Watsonia. 2000;23:93–110.

28. Bossdorf O, Auge H, Lafuma L, Rogers WE, Siemann E, Prati D. Phenotypic and genetic differentiation between native and introduced plant populations. Oecologia. 2005;144:1–11.

29. Hagenblad J, Hülskötter J, Acharya KP, Brunet J, Chabrerie O, Cousins SAO, et al. Low genetic diversity despite multiple introductions of the invasive plant species Impatiens glandulifera in Europe. BMC Genet. 2015;16:103.

30. Van Kleunen M, Weber E, Fischer M. A meta-analysis of trait differences between invasive and non-invasive plant species. Ecol Lett. 2010;13:235–45.

31. Geng Y, van Klinken RD, Sosa A, Li B, Chen J, Xu C-Y. The relative importance of genetic diversity and phenotypic plasticity in determining Invasion Success of a clonal weed in the USA and China. Front Plant Sci. 2016;7:216.

32. Richards CL, Bossdorf O, Muth NZ, Gurevitch J, Pigliucci M. Jack of all trades, master of some? On the role of phenotypic plasticity in plant invasions. Ecol Lett. 2006;9:981–93.

33. Pichancourt J-B, van Klinken RD. Phenotypic plasticity influences the size, shape and Dynamics of the Geographic distribution of an invasive plant. PLoS ONE. 2012;7:e32323.

34. Parker IM, Rodriguez J, Loik ME. An Evolutionary Approach to understanding the Biology of invasions: local adaptation and general-purpose genotypes in the weed Verbascum thapsus. Conserv Biol. 2003;17:59–72.

35. Richards CL, Walls RL, Bailey JP, Parameswaran R, George T, Pigliucci M. Plasticity in salt tolerance traits allows for invasion of novel habitat by Japanese knotweed s. l. (Fallopia japonica and F.xbohemica, Polygonaceae). Am J Bot. 2008;95:931–42.

36. Price EAC, Gamble R, Williams GG, Marshall C. Seasonal patterns of partitioning and remobilization of 14 C in the invasive rhizomatous perennial Japanese knotweed (Fallopia japonica (Houtt.) Ronse Decraene). Ecology and Evolutionary Biology of Clonal plants. Dordrecht: Springer Netherlands; 2002. pp. 125–40.

37. Bímová K, Mandák B, Pyšek P. Experimental study of vegetative regeneration in four invasive Reynoutria taxa (Polygonaceae). Plant Ecol. 2003;166:1–11.

38. Euring D, Löfke C, Teichmann T, Polle A. Nitrogen fertilization has differential effects on N allocation and lignin in two Populus species with contrasting ecology. Trees - Struct Function. 2012;26:1933–42.

39. McNear DH, Chaney RL, Sparks DL. The hyperaccumulator Alyssum murale uses complexation with nitrogen and oxygen donor ligands for Ni transport and storage. Phytochemistry. 2010;71:188–200.

40. Usman K, Al-Ghouti MA, Abu-Dieyeh MH. The assessment of cadmium, chromium, copper, and nickel tolerance and bioaccumulation by shrub plant Tetraena qataranse. Sci Rep. 2019;9:1–11.

41. Buitrago MF, Groen TA, Hecker CA, Skidmore AK. Changes in thermal infrared spectra of plants caused by temperature and water stress. ISPRS J Photogrammetry Remote Sens. 2016;111:22–31.

42. Butler HJ, Adams S, McAinsh MR, Martin FL. Detecting nutrient deficiency in plant systems using synchrotron Fourier-transform infrared microspectroscopy. Vib Spectrosc. 2017;90:46–55.

43. Butler HJ, Martin FL, Roberts MR, Adams S, McAinsh MR. Observation of nutrient uptake at the adaxial surface of leaves of tomato (Solanum lycopersicum) using Raman spectroscopy. Anal Lett. 2020;53:536–62.

44. Skolik P, McAinsh MR, Martin FL. ATR-FTIR spectroscopy non-destructively detects damage-induced sour rot infection in whole tomato fruit. Planta. 2019;249:925–39.

45. Butler HJ, McAinsh MR, Adams S, Martin FL. Application of vibrational spectroscopy techniques to non-destructively monitor plant health and development. Anal Methods. 2015;7:4059–70.

46. Skolik P, Morais CLM, Martin FL, McAinsh MR. Determination of developmental and ripening stages of whole tomato fruit using portable infrared spectroscopy and Chemometrics. BMC Plant Biol. 2019;19:236.

47. Morais CLM, Lima KMG, Singh M, Martin FL. Tutorial: multivariate classification for vibrational spectroscopy in biological samples. Nat Protoc. 2020;15:2143–62.

48. Holden CA, Morais CLM, Taylor JE, Martin FL, Beckett P, McAinsh M. Regional differences in clonal Japanese knotweed revealed by chemometrics-linked attenuated total reflection Fourier-transform infrared spectroscopy. BMC Plant Biology 2021 21:1. 2021;21:1–20.

49. Traoré M, Kaal J, Martínez Cortizas A. Differentiation between pine woods according to species and growing location using FTIR-ATR. Wood Sci Technol. 2018;52:487–504.

50. Bağcıoğlu M, Kohler A, Seifert S, Kneipp J, Zimmermann B. Monitoring of plant–environment interactions by high-throughput FTIR spectroscopy of pollen. Methods Ecol Evol. 2017;8:870–80.

51. Gordon R, Chapman J, Power A, Chandra S, Roberts J, Cozzolino D. Mid-infrared spectroscopy coupled with chemometrics to identify spectral variability in Australian barley samples from different production regions. J Cereal Sci. 2019;85:41–7.

52. Zeghoud S, Rebiai A, Hemmami H, Seghir B, Ben, Elboughdiri N, Ghareba S, et al. ATR–FTIR Spectroscopy, HPLC Chromatography, and Multivariate Analysis for Controlling Bee Pollen Quality in some Algerian regions. ACS Omega. 2021;6:4878–87.

53. Ruoff K, Luginbu¨hl W, Luginbu¨hl L, Ku¨nzli R, Ku¨nzli K, Äa M et al. Authentication of the Botanical and Geographical Origin of Honey by Mid-infrared Spectroscopy. 2006. https://doi.org/10.1021/jf060838r.

54. Met Office. UK Regional Climates. https://www.metoffice.gov.uk/research/climate/maps-and-data/regional-climates/index. 2019.

55. Bailey J. The Japanese knotweed invasion viewed as a vast unintentional hybridisation experiment. Heredity (Edinb). 2013. https://doi.org/10.1038/hdy.2012.98.

56. Smith H. Light quality, photoperception, and plant strategy. Annu Rev Plant Physiol. 1982;33:481–518.

57. Larsen DH, Woltering EJ, Nicole CCS, Marcelis LFM. Response of Basil Growth and morphology to light intensity and spectrum in a Vertical Farm. Front Plant Sci. 2020;11:1893.

58. Pennisi G, Pistillo A, Orsini F, Cellini A, Spinelli F, Nicola S, et al. Optimal light intensity for sustainable water and energy use in indoor cultivation of lettuce and basil under red and blue LEDs. Sci Hortic. 2020;272:109508.

59. Zou T, Huang C, Wu P, Ge L, Xu Y. Optimization of Artificial Light for Spinach Growth in Plant Factory Based on Orthogonal Test. Plants 2020, Vol 9, Page 490. 2020;9:490.

60. Park Y, Runkle ES. Spectral effects of light-emitting diodes on plant growth, visual color quality, and photosynthetic photon efficacy: White versus blue plus red radiation. PLoS ONE. 2018;13.

61. Monaghan RM, Paton RJ, Smith LC, Drewry JJ, Littlejohn RP. The impacts of nitrogen fertilisation and increased stocking rate on pasture yield, soil physical condition and nutrient losses in drainage from a cattle-grazed pasture. New Z J Agricultural Res. 2005;48:227–40.

62. Kuhlgert S, Austic G, Zegarac R, Osei-Bonsu I, Hoh D, Chilvers MI et al. MultispeQ Beta: a tool for large-scale plant phenotyping connected to the open photosynQ network. R Soc Open Sci. 2016;3.

63. Martin FL, et al. Distinguishing cell types or populations based on the computational analysis of their infrared spectra. Nat Prot. 2010;5:1748–60.

64. Trevisan J, Angelov PP, Scott AD, Carmichael PL, Martin FL. IRootLab: a free and open-source MATLAB toolbox for vibrational biospectroscopy data analysis. Bioinformatics. 2013;29:1095–7.

65. Morais CLM, Lima KMG. Principal Component Analysis with Linear and Quadratic Discriminant Analysis for Identification of Cancer samples based on Mass Spectrometry. Article J Braz Chem Soc. 2018;29:472–81.

66. Morais CLM, Costa FSL, Lima KMG. Variable selection with a support vector machine for discriminating: Cryptococcus fungal species based on ATR-FTIR spectroscopy. Anal Methods. 2017;9:2964–70.

67. Sharma S, Uttam KN. Rapid analyses of stress of copper oxide nanoparticles on wheat plants at an early stage by laser induced fluorescence and attenuated total reflectance Fourier transform infrared spectroscopy. Vib Spectrosc. 2017;92:135–50.

68. Nogales-Bueno J, Baca-Bocanegra B, Rooney A, Miguel Hernández-Hierro J, José Heredia F, Byrne HJ. Linking ATR-FTIR and Raman features to phenolic extractability and other attributes in grape skin. Talanta. 2017;167:44–50.

69. Talari ACS, Martinez MAG, Movasaghi Z, Rehman S, Rehman IU. Advances in Fourier transform infrared (FTIR) spectroscopy of biological tissues. Appl Spectrosc Rev. 2017;52:456–506.

70. Lei Y, Hannoufa A, Christensen D, Shi H, Prates LL, Yu P. Molecular structural changes in Alfalfa detected by ATR-FTIR spectroscopy in response to silencing of TT8 and HB12 genes. Int J Mol Sci 2018. 2018;19:19:1046.

71. Liu X, Renard CMGC, Bureau S, Le Bourvellec C. Revisiting the contribution of ATR-FTIR spectroscopy to characterize plant cell wall polysaccharides. Carbohydr Polym. 2021;262:117935.

72. Moskal P, Wesełucha-Birczyńska A, Łabanowska M, Filek M. Adaxial and abaxial pattern of Urtica dioica leaves analyzed by 2DCOS ATR-FTIR as a function of their growth time and impact of environmental pollution. Vib Spectrosc. 2019;104:102948.

73. Ord J, Butler HJ, McAinsh MR, Martin FL. Spectrochemical analysis of syca-more (Acer pseudoplatanus) leaves for environmental health monitoring. Analyst. 2016;141:2896–903.

74. Krähmer A, Böttcher C, Gudi G, Stürtz M, Schulz H. Application of ATR-FTIR spectroscopy for profiling of non-structural carbohydrates in onion (Allium cepa L.) bulbs. Food Chem. 2021;360:129978.

75. Strong R, Martin FL, Jones KC, Shore RF, Halsall CJ. Subtle effects of environ-mental stress observed in the early life stages of the common frog, Rana temporaria. Sci Rep. 2017;7:1–13.

76. Gandolfo DS, Mortimer H, Woodhall JW, Boonham N. Fourier transform infra-red spectroscopy using an attenuated total reflection probe to distinguish between Japanese larch, pine and citrus plants in healthy and diseased states. Spectrochim Acta Mol Biomol Spectrosc. 2016;163:181–8.

77. Holden C, McAinsh M, Taylor J, Beckett P, Albacele A, de Martinez-Andujar C. Morais, Camilo; Martin, Francis Attenuated total reflection Fourier-transform infrared spectroscopy for the prediction of hormone concentrations in plants. Analyst. 2024.

78. Cao Z, Wang Z, Shang Z, Zhao J. Classification and identification of Rhodo-bryum roseum limpr. And its adulterants based on fourier-transform infrared spectroscopy (FTIR) and chemometrics. PLoS ONE. 2017;12.

79. Macchioni V, Picchi V, Carbone K. Hop leaves as an alternative source of health-active compounds: Effect of genotype and drying conditions. Plants. 2022;11:99.

80. Wu H-C, Bulgakov VP, Jinn T-L. Pectin methylesterases: Cell Wall Remodel-ing proteins are required for Plant Response to heat stress. Front Plant Sci. 2018;0:1612.

81. Thalmann M, Santelia D. Starch as a determinant of plant fitness under abiotic stress. New Phytol. 2017;214:943–51.

82. Heap B, Holden C, Taylor J, McAinsh M. In: eLS, editor. <scp > ROS crosstalk in signalling Pathways</scp >. Wiley; 2020. pp. 1–9.

83. Hussain S, Iqbal N, Rahman T, Liu T, Brestic M, Safdar ME, et al. Shade effect on carbohydrates dynamics and stem strength of soybean genotypes. Environ Exp Bot. 2019;162:374–82.

84. Lemoine R. Sucrose transporters in plants: update on function and structure. Biochimica et Biophysica Acta (BBA). - Biomembr. 2000;1465:246–62.

85. Izquierdo L, Martín I, Albornos L, Hernández-Nistal J, Hueso P, Dopico B, et al. Overexpression of Cicer arietinum βIII-Gal but not βIV-Gal in arabidopsis causes a reduction of cell wall β-(1,4)-galactan compensated by an increase in homogalacturonan. J Plant Physiol. 2018;231:135–46.

86. Waldron KW, Faulds CB. Cell Wall Polysaccharides: composition and structure. Compr Glycoscience: Chem Syst Biology. 2007;1–4:181–201.

87. Dusz MA, Martin FM, Dommanget F, Petit A, Dechaume-Moncharmont C, Evette A. Review of Existing Knowledge and Practices of Tarping for the Control of Invasive Knotweeds. Plants 2021, Vol 10, Page 2152. 2021;10:2152.

88. Miller JH, Manning ST, Enloe SF. A management guide for invasive plants in southern forests. Gen Tech Rep SRS–131 Asheville, NC: US Department of Agriculture Forest Service, Southern Research Station 120 p. 2013;131:1–120.

89. Liao H, D'Antonio CM, Chen B, Huang Q, Peng S. How much do phenotypic plasticity and local genetic variation contribute to phenotypic divergences along environmental gradients in widespread invasive plants? A meta-analy-sis. Oikos. 2016;125:905–17.

90. Mounger J, Ainouche ML, Bossdorf O, Cavé-Radet A, Li B, Parepa M et al. Epigenetics and the success of invasive plants. Philosophical Trans Royal Soc B: Biol Sci. 2021;376.

91. Davidson AM, Jennions M, Nicotra AB. Do invasive species show higher phe-notypic plasticity than native species and, if so, is it adaptive? A meta-analysis. Ecol Lett. 2011;14:419–31.

92. Walls RL. Hybridization and plasticity contribute to Divergence among Coastal and Wetland populations of Invasive Hybrid Japanese Knotweed s.l. {Fallopia spp). Estuaries Coasts. 2010;33:902–18.

93. Yuan W, Pigliucci M, Richards CL. Rapid phenotypic differentiation and local adaptation in Japanese knotweed s.l. (Reynoutria japonica and R. × Bohem-ica, Polygonaceae) invading novel habitats. bioRxiv. 2022;:2022.03.07.483296.

94. da Costa VA, Tom Cothren J. Drought effects on Gas Exchange, Chloro-phyll, and Plant Growth of 1-Methylcyclopropene treated cotton. Agron J. 2011;103:1230–41.

95. Mafakheri A, Siosemardeh A, Bahramnejad B, Struik PC, Sohrabi Y. Effect of Drought stress on yield, proline and chlorophyll contents in three chickpea cultivars. Aust J Crop Sci. 2010;4:580–5.

96. Álvarez S, Bañón S, Sánchez-Blanco MJ. Regulated deficit irrigation in differ-ent phenological stages of potted geranium plants: Water consumption, water relations and ornamental quality. Acta Physiol Plant. 2013;35:1257–67.

97. Kebbas S, Lutts S, Aïd F. Effect of drought stress on the photosynthesis of Acacia tortilis subsp. raddiana at the young seedling stage. Photosynthetica 2015. 2015;53:2.

98. Hou M, Wu D, Li Y, Tao W, Chao L, Zhang Y. The role of auxin in nitrogen-modulated shoot branching. 2021;16. https://doi.org/10.1080/15592324.2021.1885888.

99. Mason MG, Ross JJ, Babst BA, Wienclaw BN, Beveridge CA. Sugar demand, not auxin, is the initial regulator of apical dominance. Proc Natl Acad Sci U S A. 2014;111:6092–7.

100. Holalu SV, Reddy SK, Finlayson SA. Low red light:Far Red Light inhibits branch-ing by promoting Auxin Signaling. J Plant Growth Regul. 2021;40:2028–36.

101. Pierik R, Cuppens MLC, Voesenek LACJ, Visser EJW. Interactions between Ethylene and Gibberellins in phytochrome-mediated shade avoidance responses in Tobacco. Plant Physiol. 2004;136:2928–36.

102. Hoad SP, Leakey RRB. Effects of light quality on gas exchange and dry matter partitioning in Eucalyptus grandis W. Hill Ex Maiden. Ecol Manage. 1994;70:265–73.

103. Jin N, Semple KT, Jiang L, Luo C, Zhang D, Martin FL. Spectrochemical analy-ses of growth phase-related bacterial responses to low (environmentally-relevant) concentrations of tetracycline and nanoparticulate silver. Analyst. 2018;143:768–76.

104. Kharrat F, Khlif M, Hilliou L, Haboussi M, Covas JA, Nouri H, et al. Minimally processed date palm (Phoenix dactylifera L.) leaves as natural fillers and processing aids in poly(lactic acid) composites designed for the extrusion film blowing of thin packages. Ind Crops Prod. 2020;154:112637.

105. Chiang C, Olsen JE, Basler D, Bånkestad D, Hoch G. Latitude and weather influences on sun light quality and the relationship to tree growth. Forests. 2019;10.

106. Kotilainen T, Aphalo PJ, Brelsford CC, Böök H, Devraj S, Heikkilä A, et al. Pat-terns in the spectral composition of sunlight and biologically meaningful spectral photon ratios as affected by atmospheric factors. Agric Meteorol. 2020;291:108041.

107. Durand M, Murchie EH, Lindfors AV, Urban O, Aphalo PJ, Robson TM. Diffuse solar radiation and canopy photosynthesis in a changing environment. Agric Meteorol. 2021;311:108684.

108. Ballaré CL, Pierik R. The shade-avoidance syndrome: multiple signals and ecological consequences. Plant Cell Environ. 2017;40:2530–43.

109. Martin F-M, Dommanget F, Janssen P, Spiegelberger T, Clément V, ·, Evette A. Could knotweeds invade mountains in their introduced range? An analysis of patches dynamics along an elevational gradient. Alp Bot. 2019;129:33–42.

110. Dommanget F, Spiegelberger T, Cavaillé P, Evette A. Light availability prevails over soil fertility and structure in the performance of Asian knotweeds on riv-erbanks: new management perspectives. Environ Manage. 2013;52:1453–62.

111. Vohland M, Ludwig B, Seidel M, Hutengs C. Quantification of soil organic carbon at regional scale: benefits of fusing vis-NIR and MIR diffuse reflectance data are greater for in situ than for laboratory-based modelling approaches. Geoderma. 2022;405:115426.

112. Fernández-Novales J, Tardaguila J, Gutiérrez S, Marañón M, Diago MP. In field quantification and discrimination of different vineyard water regimes by on-the-go NIR spectroscopy. Biosyst Eng. 2018;165:47–58.

113. Diago MP, Bellincontro A, Scheidweiler M, Tardaguila J, Tittmann S, Stoll M. Future opportunities of proximal near infrared spectroscopy approaches to determine the variability of vineyard water status. Aust J Grape Wine Res. 2017;23:409–14.

114. Diago MP, Fernández-Novales J, Gutiérrez S, Marañón M, Tardaguila J. Devel-opment and validation of a new methodology to assess the vineyard water status by on-the-go near infrared spectroscopy. Front Plant Sci. 2018;9:59.

115. Pandey P, Ge Y, Stoerger V, Schnable JC. High throughput in vivo analysis of plant leaf chemical properties using hyperspectral imaging. Front Plant Sci. 2017;8:1348.

116. Bureau S, Cozzolino D, Clark CJ. Contributions of Fourier-transform mid infrared (FT-MIR) spectroscopy to the study of fruit and vegetables: a review. Postharvest Biol Technol. 2019;148:1–14.

117. Hutengs C, Seidel M, Oertel F, Ludwig B, Vohland M. In situ and laboratory soil spectroscopy with portable visible-to-near-infrared and mid-infrared instruments for the assessment of organic carbon in soils. Geoderma. 2019;355:113900.

118. Ji W, Adamchuk VI, Biswas A, Dhawale NM, Sudarsan B, Zhang Y, et al. Assessment of soil properties in situ using a prototype portable MIR spectrometer in two agricultural fields. Biosyst Eng. 2016;152:14–27.

119. Dhawale NM, Adamchuk VI, Prasher SO, Viscarra Rossel RA, Ismail AA, Kaur J. Proximal soil sensing of soil texture and organic matter with a prototype portable mid-infrared spectrometer. Eur J Soil Sci. 2015;66:661–9.

120. Soriano-Disla JM, Janik LJ, McLaughlin MJ. Assessment of cyanide contamination in soils with a handheld mid-infrared spectrometer. Talanta. 2018;178:400–9.

121. Jones D, Bruce G, Fowler MS, Law-Cooper R, Graham I, Abel A, et al. Optimising physiochemical control of invasive Japanese knotweed. Biol Invasions. 2018;20:2091–105.

122. Martin FM, Müllerová J, Borgniet L, Dommanget F, Breton V, Evette A. Using Single- and Multi-Date UAV and Satellite Imagery to Accurately Monitor Invasive Knotweed Species. Remote Sensing. 2018, Vol 10, Page 1662. 2018;10:1662.

Publisher's Note